Available online at www.sciencedirect.com
ScienceDirect
Journal of Photochemistry and Photobiology A: Chemistry 192 (2007) 66–73
Journal of Photochemistry and Photobiology A:Chemistry
www.elsevier.com/locate/jphotochem

Sterically tuned photoreactivity of an aromatic α-diketone family

Jean-Pierre Malval, Céline Dietlin, Xavier Allonas *, Jean-Pierre Fouassier

Département de Photochimie Générale UMR CNRS 7525, Université de Haute Alsace, ENSCMu 3 rue Alfred Werner, 68093 Mulhouse, France

Received 7 March 2007; received in revised form 27 April 2007; accepted 1 May 2007
Available online 5 May 2007

Abstract

The photophysics and photochemistry of five aromatic α-diketones exhibiting different geometries are reported. The ground state geometry is correlated to the absorption spectra and electron reduction properties. The emissive singlet states of transoidal α-diketones have a n,π* character and are weakly polar. The triplet states of all α-diketones exhibit a strong n,π* character which is consistent with the vibronic structure of the phosphorescence spectrum observed both in glassy matrix at 77 K and in oxygen-free solution at room temperature. The triplet state energies are influenced by the *trans*/*cis* conformation and by the degree of conjugation of the carbonyl groups with their adjacent phenyl moities. These two factors have important consequences on the α-diketone photoreactivities. The reaction constants ρ of the Hammett's plot for the triplet state quenching by several phenol derivatives indicate that the electrophilic character of the transient state is tunable by rotation of the intercarbonyl dihedral angle. After hydrogen abstraction, the intramolecular hydrogen exchange between the two vicinal carbonyl groups plays a major role in the stabilization of the produced ketyl radical. Consequently, the rate constants of hydrogen abstraction in the presence of 2-propanol vary by three orders of magnitude.

Keywords: Diketones; Excited states; Phosphorescence; Fluorescence; Conformation

1. Introduction

Spectroscopic and electronic properties of α-diketones have been the subject of an important number of theoretical and experimental studies [1–9]. Such compounds have demonstrated their versatile use in many applications such as in the photoepoxidation of olefins in the presence of oxygen [10–12] or as photoinitiators of free radical polymerization when associated with an hydrogen donor [13–15]. For instance, camphorquinone in connection with a tertiary amine is widely used as a free oxygen two-component photocuring system for acrylate-based dental restorative resins [16,17]. In that case, the photoinitiating process generally occurred via a triplet excited state T_1 [18]. Obviously, the photoreduction of the α-diketone triplet state mainly influences the efficiency of the primary process. This photoreduction is subsequently governed by several intrinsic factors such as: (i) the triplet energy level E_T which explains for instance that benzophenone ($E_T = 69$ kcal mol^{-1}) is 1000 times more photoreducible than biacetyl ($E_T = 56$ kcal mol^{-1}) in the presence of isopropanol; (ii) the π,π* or n,π* character of the T_1 state which directs the electron density localization at the excited state and then the symmetry of the transition state; (iii) the reactivity of the T_1 state toward the hydrogen abstraction reaction that can be "switched-off" due to an electron donating contribution of the heteroatom placed at the α position of a carbonyl function [19,20] (this was recently exemplified through the measurement of the relative photoreduction rates of *N*-methylisatin and 3,3 dimethyl-1,2-indanedione and explained on the basis of an excited charge transfer process which decreases the electrophilicity of the carbonyl oxygen [21]); (iv) the geometry conformation which is expected to be a key factor to modulate the photoreactivity of the excited states.

Among the large number of sterical parameters that influence the electronic properties of the α-diketone chromophores, some of them are mainly decisive to describe the photophysical properties: for example, several working groups have clearly demonstrated that the n,π* nature of the lowest singlet and triplet states is strongly dependent on the intercarbonyl dihedral angle [3,7,8,22–24]. However, this photorotamerism approach on the T_1 state has been poorly correlated to the photoreactivity.

* Corresponding author. Tel.: +33 389 33 50 11; fax: +33 389 33 50 14.
E-mail address: xavier.allonas@uha.fr (X. Allonas).

1010-6030/$ – see front matter © 2007 Elsevier B.V. All rights reserved.
doi:10.1016/j.jphotochem.2007.05.005

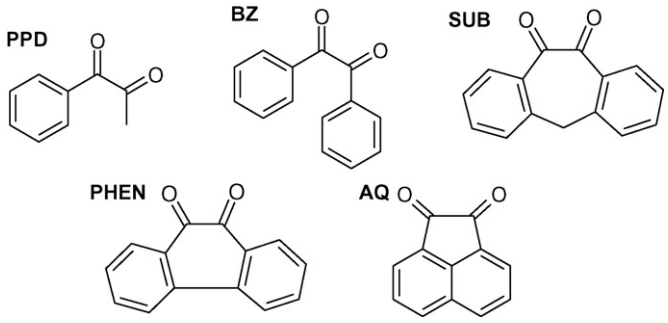

Scheme 1. Formulas of the studied α-diketones.

The present article is devoted to a study of a carefully selected aromatic α-diketone family (Scheme 1). The main goal of this paper is to correlate the photophysical and photochemical properties of these compounds to the geometry conformations of the ground and excited states. Relevant parameters that strongly influence the photoreactivity of such a α-diketone family will be highlighted.

2. Experimental and methodology

All the solvents employed were Aldrich or Fluka spectroscopic grade. Dibenzo[*a*,*d*]cyclohepta[1,4]-diene-10,11-dione (SUB) was a gift from Dr D. Lougnot. 1-Phenyl-1,2-propanedione (PPD), benzil (BZ), 9,10-phenanthrenequinone (PHEN), acenaphtenequinone (AQ) as well as the phenol derivatives, triethylamine and 2-propanol were purchased from Aldrich. Except for AQ (which was recrystallized from acetic acid and kept in the dark to prevent photooxidation to 1,8-naphtalic anhydride), all compounds were used without any further purification.

The cyclic voltammetry experiments (using a computer-controlled Princeton 263A potentiostat with a three-electrode single-compartment cell; a saturated calomel electrode in methanol used as a reference was placed in a separate compartment) were performed at 300 K, in Ar-degassed acetonitrile with a constant concentration (0.1 M) of n-Bu_4BF_4. Ferrocene was used as an internal reference.

The UV–vis spectra were recorded in a Beckman DU-640. The oscillator strengths f of the S_0–S_1 electronic transition were calculated using the following relationship [18]: $f = 4.10^{-9}$ $(\varepsilon \Delta \nu_{1/2})/2$, where ε (M^{-1} cm^{-1}) and $\Delta\nu_{1/2}$ (cm^{-1}) correspond to the extinction coefficient of the transition and its corresponding half band width, respectively. For PHEN, a set of Gaussian functions were necessary to deconvolve the absorption band.

A FluroMax 2 Luminescence Spectrometer was used for the fluorescence and phosphorescence measurements. All the fluorescence spectra were spectrally corrected; the fluorescence quantum yields (which took into account the correction due to the solvent refractive index) were determined relatively to quinine bisulfate in 0.1N sulfuric acid ($\phi = 0.52$) [25]. The fluorescence lifetimes were measured using, as an excitation source, a pulsed diode laser emitting at 372 nm operated by diode controller (PDL-800-B, Picoquant) operating at 40 MHz. The detection was based on a fast photomultiplier (H5783P-04, Hamamatsu) and a single photon counting setup (Fluotime 100 and Timeharp 200, Picoquant). The response function was lower than 0.1 ns and a classical procedure of iterative deconvolution was applied. Steady-state anisotropy measurements were performed in 2-methyltetrahydrofuran at 77 K. The samples are placed in a 5-mm diameter quartz tube inside a Dewar filled with liquid nitrogen. Two Glan–Thompson polarizers are placed in the excitation and emission beams. The anisotropy r is determined as follows:

$$r = \frac{I_{VV} - gI_{VH}}{I_{VV} + 2gI_{VH}} \quad \text{with } g = \frac{I_{HV}}{I_{HH}}$$

where I is the fluorescence intensity. The subscripts denote the orientation (horizontal H or vertical V) of the excitation and emission polarizers, respectively. g is an instrumental correction factor. The phosphorescence spectra were collected at room temperature in deaerated acetonitrile by bubbling oxygen-free argon for 20 min. Each spectrum is discriminated from fluorescence by subtracting the spectra collected after and before degassing.

Laser flash photolysis (LFP) experiments were carried out with a Edinburgh Analytical Instruments LP900 equipped with a 450-W pulsed Xe arc lamp, a Czerny-Turner monochromator and a fast photomultiplier. Samples previously deaerated were irradiated with the third harmonic ($\lambda = 355$ nm, pulse duration about 10 ns, 5 mJ $pulse^{-1}$) of a Nd/YAG (Powerlite 9010, Continuum). Sample concentration was adjusted to get an absorption of 0.3 at the excitation wavelength.

Molecular modelling was performed with Gaussian 03 running on the 16 processor cluster (16 Itanium 1.8 GHz, Altix, Silicon Graphics) of the laboratory. Optimization of the ground state structures was performed with both HF/6-31+G* and B3LYP/6-31+G* methods. Electronic transitions were computed on the optimized geometries using a time-dependent method B3LYP/6-311++G** [26].

3. Results and discussion

3.1. Ground state properties

The absorption spectra of the studied α-diketones in acetonitrile are depicted in Fig. 1. The experimental and theoretical data are listed in Table 1. PPD and BZ exhibit absorption spectra similar in shape between 220 and 350 nm. They are intense and correspond to allowed $\pi\pi^*$ transitions. They consist into a main band localized at 255 nm and a shoulder at 285 nm which correspond to the S_0–^1L_a and S_0–^1L_b transitions (according to the Platt notations for the L_a and ^1L_b states [27]) centred on the acetophenyl moities. Interestingly, these two bands which are invariant to the solvent polarity exhibit extinction coefficients twice higher for BZ than for PPD. The benzoyl fragments of benzil thus appear as electronically decoupled in the ground state. This decoupling is consistent with the high intercarbonyl dihedral angles $\phi_{CO–CO}$ derived from optimized geometries at the HF/6-31+G* and B3LYP/6-31+G* levels of theory. Although both methods give different values, the same trends are observed. Indeed, the $\phi_{CO–CO}$ values exceed 90°, indicating that both PPD and BZ exhibit a transoidal conformation. As a consequence of

Table 1
UV absorption spectral data, calculated intercarbonyl dihedral angles and reduction potentials of α-diketones

	λ_{abs} (nm)	ε[a] ($M^{-1}\,cm^{-1}$)	$\Delta\nu_{1/2}$[a] (cm^{-1})	f (×100)	ϕ_{CO-CO} (°)[b]	ϕ_{CO-CO} (°)[c]	E_{red}[a] (mV/Fc)
PPD	391[a]; 444[d]	34	6000	0.082[a]; 0.05[c]	116	135	−1400[e]
BZ	378[a]; 428[d]	80	4250	0.13[a]; 0.06[c]	136	116	−1250
SUB	434[a]; 478[d]	67	1875	0.050[a]; 0.01[d]	41.2	25.9	−985
PHEN	495[a]; 554[d]	40	1150	0.018[a]; 0.00[d]	11.3	0.02	−720
AQ	478[a]; 535[d]	27	2200	0.024[a]; 0.00[c]	0.00	0.00	−1000

[a] In acetonitrile.
[b] Optimized at the HF/6-31+G* level.
[c] Optimized at the B3LYP/6-31+G* level.
[d] Computed at the TD B3LYP/6-311++G** level on the optimized B3LYP/6-31+G* geometry.
[e] Irreversible.

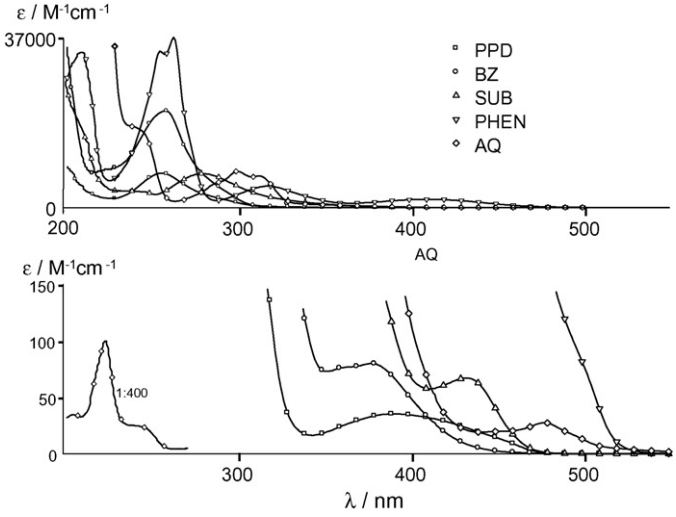

Fig. 1. Absorption spectra of the α-diketones in acetonitrile: (□) PPD, (◯) BZ, (△) SUB, (▽) PHEN, (◇) AQ.

the carbonyl group decoupling, the reduction potentials of these compounds (Table 1) are comparable to that of benzaldehyde (−1400 versus Fc^+/Fc) [28]. The non reversible voltammograms obtained for PPD show that the radical anion is destabilized by the methyl group (+I effect), confirming indirectly the role of the two ketone moities in the delocalization of the negative charge.

In contrast, the lowest energy electronic transitions have extinction coefficients which do not exceed 100 $M^{-1}\,cm^{-1}$ with oscillator strengths lower than 0.01: they are strongly forbidden. An hypsochromy is noted with a shift that is about 10 nm for BZ when going from cyclohexane to acetonitrile and 17 nm for PPD. Both the extinction coefficients and the solvatochromy are in line with $n\pi^*$ transitions. The extinction coefficient of the lowest energy absorption band is twice higher for BZ than for PPD. This underlines that the enhancement of the steric hindrance around the intercarbonyl bond for BZ compared to PPD leads to a lower conformer dispersion and consequently explains the noticeable increase of the oscillator strength and a substantial narrowing of the last absorption band.

The absorption spectrum of SUB consists in a large band centred at 275 which lies up to 380 nm. The S_0–S_1 absorption band around 430 nm exhibits a blue shift in different solvents of increasing polarity. The maximum absorption wavelength increases by 10 nm from cyclohexane to acetonitrile. While ϕ_{CO-CO} strongly decreases from BZ to SUB, a similar blue shift is observed when going to higher polarity solvents. As usually stated for rotation effects around a chemical bond [29], this clearly indicates that the difference between the dipole moments of the ground state and the Franck–Condon excited state is maintained constant upon the rotation of the intercarbonyl bond.

Comparison of the absorption spectrum of PHEN with phenanthrene used as model shows an important change. Phenanthrene exhibits an intense S_0–^1B_a transition and two weak S_0–^1L_a and S_0–^1L_b transitions at 290 nm and 330 nm [27]. In PHEN, the S_0–^1B_a transition is red shifted to 265 nm. The S_0–^1L_a and S_0–^1L_b transitions are not discernable any more as two new large bands are observed at 320 and 415 nm. These bands are sensitive to the solvent polarity as they are red shifted by 7 and 17 nm, respectively, when changing cyclohexane for acetonitrile. Time-dependent density functional theory computations (at the TD-B3LYP/6-311++G** level) on the full geometrical optimized structure of PHEN clearly show that these two bands exhibit a charge transfer CT character going from the phenanthrene (donor) to the biacetyl fragment (acceptor). This is consistent with the fact that the progressive addition of trifluoroacetic acid to an acetonitrile solution of PHEN induces a red shift of these two bands. This red shift is attributable to the fact that the oxygen protonation of the carbonyl groups leads to a positive charge formation on the dicarbonyl subsystem which increases its electron acceptor character and therefore favours the CT process.

Similar results are found with AQ when compared with naphthalene. The intense band at 300 nm corresponding to the ^1L_a transition [30] keeps its vibronic structure but is red shifted by 25 nm. Moreover, a large shoulder appears at the red tail, it was assigned to a $\pi \rightarrow \pi^*$ transition which involves an electron redistribution between the naphthalene and the dicarbonyl moiety and also exhibits a CT character [31].

The progressive decrease of ϕ_{CO-CO} from PPD to AQ leads to a cisoidal geometry for SUB, PHEN and AQ. As a consequence, the aromatic conjugation between the phenyl moities is favoured and leads to a red shift of the S_0–S_1 band. This conformational change has also a strong consequence on the α-diketone reduction potential which is very sensitive to the decoupling of the two benzene rings. From PPD to PHEN, the $E^{red}_{1/2}$ values increase with decreasing ϕ_{CO-CO}, showing that the

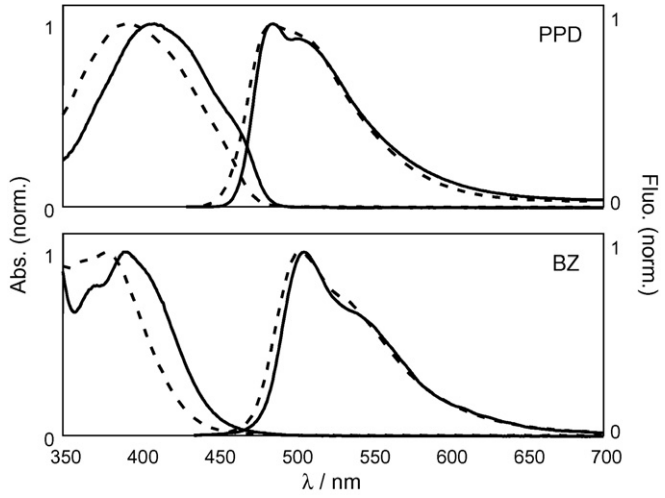

Fig. 2. Normalized absorption and fluorescence spectra of PPD and BZ in cyclohexane (full lines) and in acetonitrile (dashed lines).

coplanarity of the two carbonyl groups enhances the electron acceptor character. The reduction potentials not only measure the relative electron acceptor ability of this aromatic α-diketone series but also give a qualitative test for the degree of conjugation of the carbonyl fragments of each molecule. In our case, a pre-organisation of the α-diketones into a cisoidal conformation appears as a favourable factor for an amplification of the electron acceptor capability in the ground state.

Time-dependent computations at the TD-B3LYP/6-311++G** level and in the gas phase predict first electronic transitions to be 53 nm red-shifted compared to the experimental maximum absorption bands. This corresponds to about 10% error in energy. This electronic transition is strongly forbidden for all the structures with oscillator strengths lower than 0.01. The predicted oscillator strengths are in good agreement with the experimental ones, with values lower than 0.01, and a good trend over the whole series of molecules.

3.2. Excited state properties

3.2.1. Fluorescence emission

The fluorescence is collected upon exciting at the maximum absorption wavelength of the S_0–S_1 absorption band. SUB, PHEN and AQ do not exhibit any fluorescence whatever the solvent used. Fig. 2 displays the emission spectra of PPD and BZ in cyclohexane and in acetonitrile. Even in a polar solvent such as acetonitrile, the fluorescence bands of PPD and BZ show vibrational structures which are associated to a symmetrical intercarbonyl bond stretching mode. The respective wave numbers (950 and 1150 cm^{-1}) are consistent with the values measured from the I.R. spectra [22]. The large distribution of rotamers observed in the ground state of PPD [3] does not appear any more in the first excited state: indeed, the fluorescence half-band widths of PPD and BZ are of the same order whatever the solvent. The very large Stokes-shift between the absorption and the fluorescence and the absence of a mirror image relationship denote a significant geometry relaxation between the ground state and excited state conformations. The fluorescence spectra do not change upon increasing the solvent polarity: compared to the blue shift of the S_0–S_1 absorption band, this indicates that the radiative deactivation of the S_1 state occurs only from a well defined and weakly polar geometrical structure. Planar transoidal (for example in PPD and BZ) and cisoidal conformations were proposed as possible geometric skewed structures of excited species [23]. The transoidal hypothesis is clearly consistent with the present observations since it requires a large twisting of the intercarbonyl bond and leads to a decrease of the excited state dipole moment due to the C_{2h} symmetry of this conformation.

Table 2
Fluorescence spectroscopic data of PPD and BZ

	λ_{fluo} (nm)	$\phi_{fluo} \times 10^3$	τ_{fluo} (ns)	k_r (s^{-1})	k_r^{cal} (s^{-1})	k_{nr} (s^{-1})
PPD	482	1.3	2.6	5×10^5	5.4×10^5	3.8×10^8
BZ	502	2.5	2.2	1.1×10^6	9.5×10^5	4.5×10^8

Excitation at the maximum absorption wavelength of the S_0–S_1 absorption band.

The fluorescence lifetimes in acetonitrile are given in Table 2. All compounds exhibit a mono-exponential decay. From the fluorescence lifetimes (τ_{fluo}) and the quantum yields (ϕ_f), both the radiative k_r and non-radiative k_{nr} (intersystem crossing plus internal conversion processes) rate constants can be derived. Calculated k_r values can also be derived from the relationship: $k_f^{cal} = \nu_0^2 f$ where ν_0 (in cm^{-1}) and f are the wavelength number and the oscillator strength of the S_0–S_1 transition, respectively. Table 2 shows that the calculated and experimental values are in good agreement. The radiative rate constants are very low and do not exceed 10^6 s^{-1}. Large k_{nr} values (more than 400 times higher than k_r) are noted. This is in agreement with the contention that $n\pi^*$ S_1 states are very weakly emissive excited states and usually present a high intersystem crossing rate constant.

Table 3
Phosphorescence spectroscopic data of α-diketones in acetonitrile

	2MeTHF ($T = 77$ K)		ACN ($T = 300$ K, O_2 free)				
	E_T (kcal mol^{-1})	ν (cm^{-1})	E_T (kcal mol^{-1})	ν (cm^{-1})	$\Delta E_{S_1-T_1}$ (kcal mol^{-1})	λ_{abs} (T_1–T_n) nm)	τ_T (ns)
PPD	53.9	1540	52.9	1450	6.5	450	4900
BZ	53.8	1470	50.9	1640	6.0	480	450
SUB	56.5	1580	–	–	–	420	110
PHEN	51.5	1570	49.7	1480	4.4	460	2700
AQ	51.9	1620	50.4	1640	3.8	600	4200

See text. Triplet state lifetimes τ_T.

3.2.2. Phosphorescence emission

Fig. 3A shows the phosphorescence spectra recorded in a glassy matrix of 2-methyltetrahydrofuran at 77 K. Each spectrum unambiguously reveals a strong vibronic structure that can be associated with symmetrical carbonyl stretching modes (wave numbers ranging from 1450 to 1650 cm^{-1}). The phosphorescence band shapes are typical of emissive triplet states having a strong n,π^* character.

Table 3 gathered the triplet energies calculated from the phosphorescence maximum wavelength for each diketone: these energies values are close to those previously measured for BZ, PPD by phosphorescence and PHEN, AQ by laser spectroscopy [21,23,32–34]. The triplet states of PPD and BZ on one hand, PHEN and AQ on the other hand exhibit similar energies around 53.8 and 51.7 kcal mol^{-1}, respectively. This is explained by the very close geometry of each respective triplet state: for the two latter cyclic diketones, the rigid and planar cisoidal conformation can be obviously invoked. Moreover, the electronic delocalization of the oxygen unpaired electrons is also a stabilizing factor that well explains the low value of the triplet energy. The more flexible transoidal conformations for PPD and BZ lead to a slightly higher energy. SUB is characterised by a triplet energy of 56.5 kcal mol^{-1}. The geometry of SUB is cisoidal but contrary to PHEN or AQ, the oxygen atoms do not participate to the conjugation any more. A flexibility increase around a carbonyl group leads to a more pronounced aliphatic character and an increase of E_T [36]: this holds true for SUB where the seven member ring imparts more flexibility.

In the case of BZ only, the phosphorescence spectrum is dependent on the excitation wavelength, as shown in Fig. 4. When the excitation moves from 430 to 380 nm, the phosphorescence emission is blue shifted by 20 nm corresponding to a significant triplet energy increase of 2.1 kcal mol^{-1}. The excitation spectra recorded at the blue and red edge of the phosphorescence spectrum, respectively, reveal the existence of two

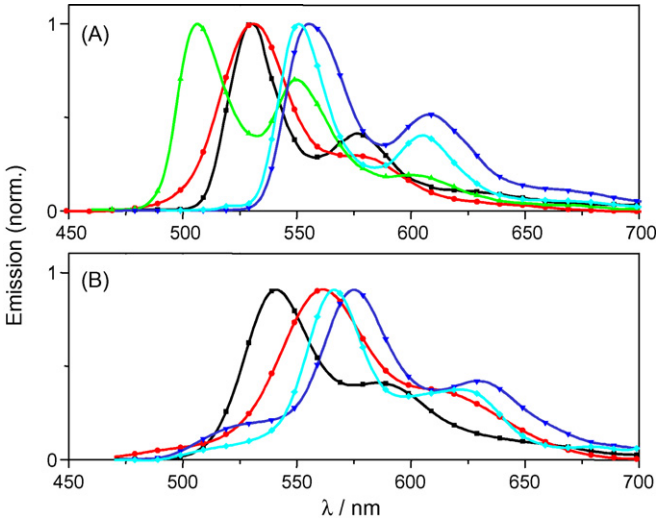

Fig. 3. (A) Phosphorescence spectra of the α-diketones in a glassy matrix of 2-methyltetrahydrofuran at 77 K/(■) PPD, (●) BZ, (▲) SUB, (▼) PHEN, (◄) AQ. (B) Phosphorescence spectra of the α-diketones in oxygen-free acetonitrile at 300 K/(■) PPD, (●) BZ, (▼) PHEN, (◄) AQ.

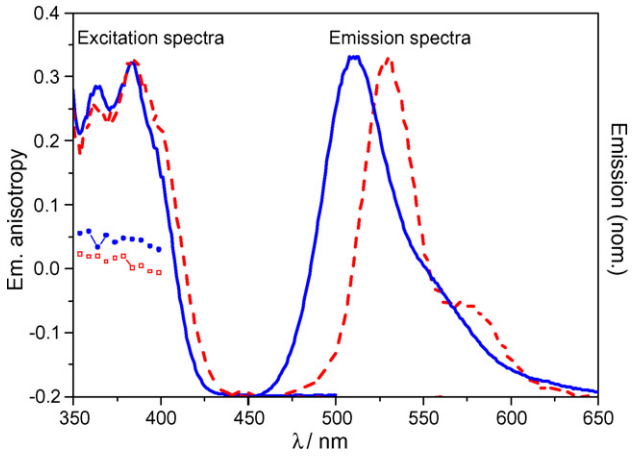

Fig. 4. Emission spectra, excitation spectra and anisotropy of the excitation spectra of BZ in a glassy matrix of 2-methyltetrahydrofuran. (i) Full lines (λ_{exc}: 380 nm and λ_{em}: 470 nm)/(●) anisotropy of the excitation spectrum collected at 470 nm; (ii) dashed lines (λ_{exc}: 430 nm and λ_{em}: 580 nm); (iii)/(□) anisotropy of the excitation spectrum collected at 580 nm.

excited species populations (Fig. 4): the decay time is 4.70 ms when exciting at 390 and 5.34 ms when exciting at 430 nm. This behaviour was already shown for BZ, the blue emitting species presenting a geometrical structure similar to that of the SUB triplet state [34,35].

While their excitation spectra are very similar, the red emitting species exhibit a noticeable red absorption band tail. Steady state anisotropy measurements also enable to discriminate these two species: the blue and red emitting species have an average anisotropy of 0.038 and 0.003, respectively. The former anisotropy is equivalent to that measured for SUB (0.032), besides the triplet energies are also similar: this confirms that the blue emitting species BZ and SUB triplet states present a similar geometrical structure.

At room temperature (except for SUB which is non phosphorescent in that case), all diketones still exhibit vibronic structured emission spectra (Fig. 3B). The excitation wavelength effect is not observed any more for BZ. Moreover, a shoulder in the blue region of the phosphorescence spectra is noted: in the case of BZ, this emission was attributed to the delayed fluorescence that is usually generated by a thermally activated reverse intercrossing system between the lowest singlet and triplet states [32,33,37]. The energy gaps between S_1 and T_1 are listed in Table 3: they do not exceed 10 kcal/mol which is a characteristic of $S_1(n,\pi^*)$–$T_1(n,\pi^*)$ splitting [21,23,32–34].

3.2.3. Triplet states reactivity

The transient absorption spectra of α-diketones were recorded after laser excitation in deaerated acetonitrile. Fig. 5 shows the spectrum obtained for SUB. Under our experimental conditions and at low light energy excitation (~4 mJ $pulse^{-1}$), triplet–triplet annihilation can be avoided so that each triplet-state absorption decay can be fitted with a first-order kinetics (the triplet lifetimes are collected in Table 3). Except for AQ, all aromatic α-diketones exhibit a strong absorption band between 400 and 550 nm. The T_1–T_n absorption spectra of PPD and BZ present a maximum at 450 nm and 480 nm, respectively

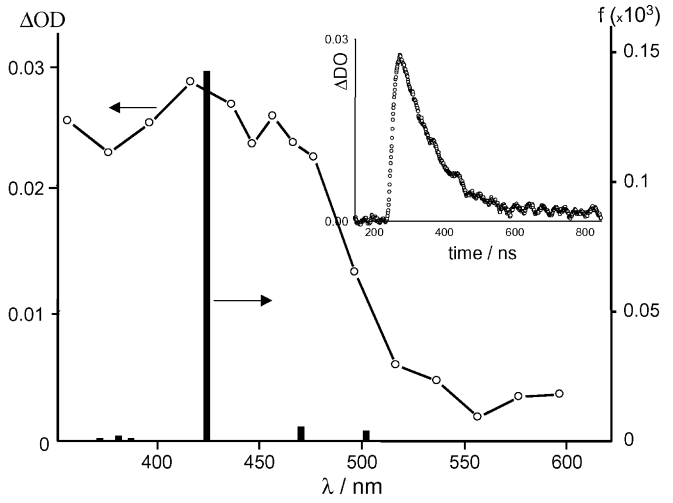

Fig. 5. Experimental triplet–triplet absorption spectrum of SUB taken 300 ns after the laser pulse in oxygen-free acetonitrile. Excitation: 355 nm. Insert: decay of the transient at 410 nm. Calculated triplet–triplet absorption spectrum.

[38]. The cyclic aromatic α-diketones have a T_1–T_n maximum wavelength that shifts to the red region and a triplet lifetime that increases when the aromaticity is increased (e.g. SUB and AQ). Time-dependent computation at the B3LYP/6-311++G** level on the relaxed triplet state allows to predict many T_1–T_n transitions, the lowest having absorption in the near IR. This underlines that upper triplet states are very close to T_1. Beyond this fact, the prediction is in good agreement with the experiments, as shown in Fig. 5 in the case of SUB triplet state absorption spectrum.

The interaction of the α-diketone triplet states with quenchers having hydrogen and electron donor character such as 2-propanol, triethylamine TEA and some phenol derivatives was investigated. This leads to the formation of a ketyl radical as shown for SUB in Fig. 6. The latter spectrum exhibits a maximum absorption located at 380 nm with a broad shoulder in the 450 nm wavelength range, in perfect agreement with the calculated spectrum at the B3LYP/6-311++G** level. This underlines

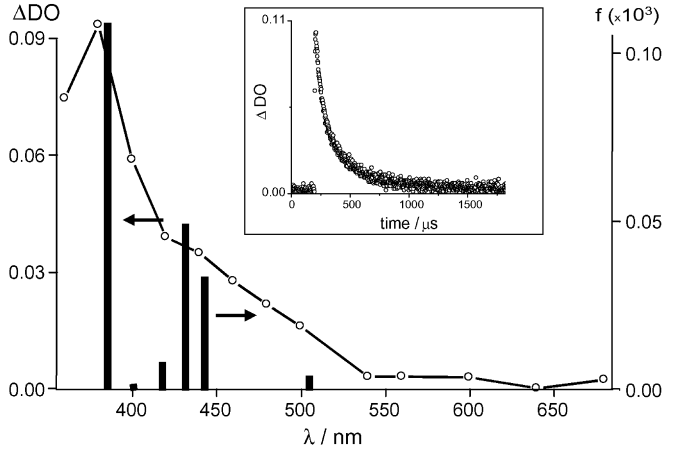

Fig. 6. Experimental and calculated transient absorption spectra of the ketyl radical of SUB in oxygen-free acetonitrile (1 μs after laser pulse). Excitation: 355 nm. Insert: decay of the transient monitored at 380 nm. Calculated ketyl radical absorption spectrum.

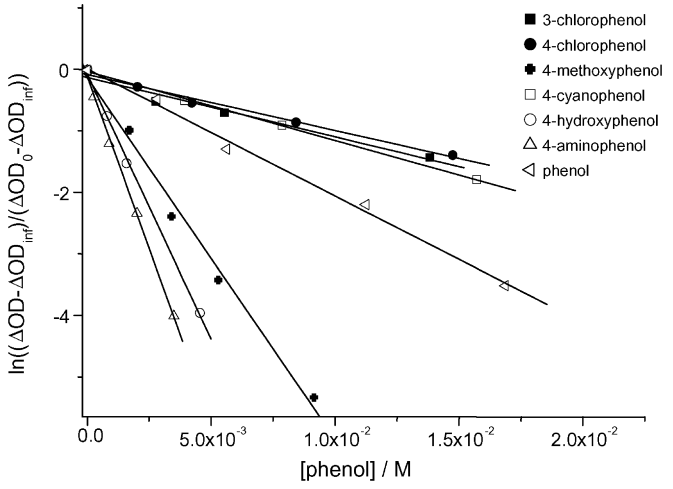

Fig. 7. Quenching plots for the SUB triplet state/phenol derivatives interaction in oxygen-free acetonitrile (λ_{exc}: 355 nm, λ_{ana}: 460 nm).

again how well TDDFT methods can be used for the prediction of radical spectra.

Interaction rate constants k_q are usually obtained by following the triplet state decay k_{exp} according to the Stern–Volmer equation: $k_{exp} = k_0 + k_q[Q]$, where k_0 is the decay rate constant of the triplet state in absence of quencher and $[Q]$ is the quencher concentration. The ketyl absorption sometimes prevented such a measurement and therefore the following treatment was used. As the triplet state disappears with the same kinetics as the ketyl radical is formed, the k_{exp} rate constant can be obtained from the following relationship [39]:

$$\ln \frac{\Delta OD - \Delta OD_\infty}{\Delta OD_0 - \Delta OD_\infty} = -k_{exp} t$$

where ΔOD is the transient absorption at time t, ΔOD_0 the absorption just after the pulse and ΔOD_∞ is the final absorption. Fig. 7 shows typical representative plots for the quenching of SUB by several phenols.

Rate constants k_q are gathered in Table 4. The triplet states of PPD and BZ are quite insensitive to 2-propanol even in pure 2-propanol solution, the upper limit value ($<1.7 \times 10^4\ M^{-1}\ s^{-1}$) being similar to that of biacetyl [40]. In the opposite way, SUB exhibits the highest rate constant of the cisoid diketones

Table 4
Rate constants of the interaction between the α-diketones and various hydrogen donors in acetonitrile

Quenchers	k_q ($M^{-1}\ s^{-1}$)				
	PPD	BZ	SUB	PHEN	AQ
4-Aminophenol	7.1×10^9	6.8×10^9	1.1×10^{10}	1.0×10^{10}	1.1×10^{10}
4-Hydroxyphenol	8.4×10^8	1.3×10^9	7.7×10^9	5.2×10^9	4.1×10^9
4-Methoxyphenol	2.9×10^8	1.1×10^9	5.7×10^9	8.3×10^9	3.8×10^9
Phenol	2.5×10^6	3.5×10^6	1.2×10^9	9.1×10^8	7.1×10^7
4-Chlorophenol	5.1×10^6	7.4×10^6	8.8×10^8	1.2×10^9	5.6×10^7
3-Chlorophenol	5.7×10^5	1.0×10^6	9.4×10^8	5.6×10^8	4.5×10^7
4-Cyanophenol	4.6×10^5	1.3×10^6	8.5×10^8	3.9×10^8	8.6×10^6
Triethylamine	2.3×10^8	6.3×10^8	8.7×10^9	3.1×10^9	4.0×10^9
2-Propanol	$<1.7 \times 10^4$	$<1.7 \times 10^4$	2.7×10^7	4.7×10^6	1.2×10^5

Table 5
The ρ values in the Hammett's plots for the hydrogen abstraction of the α-diketone triplet states by phenol derivatives

PPD	BZ	SUB	PHEN	AQ
-2.23 ± 0.15 (0.98)[a]	-2.14 ± 0.19 (0.98)[a]	-0.65 ± 0.07 (0.97)[a]	-0.77 ± 0.07 (0.98)[a]	-1.63 ± 0.11 (0.99)[a]

[a] Linear regression coefficient.

(2.7×10^7 M^{-1} s^{-1}). However, the rate constant for PHEN and AQ is about 6 and 200 times lower, respectively.

Quenching rate constants of PPD and BZ by TEA roughly correspond to that of biacetyl [40]. The poor linear correlation ($r = 0.80$) obtained when plotting log k_q versus the diketones reduction potentials E_{red} might indicate that the primary charge transfer process is not the driving one and indirectly confirms that excited states exhibiting a n,π^* character are less sensitive to open shell charge acceptor ability.

Phenolic hydrogen abstraction reactions produce a phenoxyl and a ketyl radical. The quenching rate constants are strongly dependent on the α-diketone (for example, for PPD, k_q increases by a factor of 10000 from 4-cyanophenol to 4-aminophenol; this factor is about 15 for SUB). The linear Hammett plots of the interaction rate constants of the α-diketones as a function of the various *para*- and *meta*-substituted phenols are depicted in Fig. 8. A better correlation is obtained when using σ^+ values rather than σ values as usually done [41]. The reaction constant values ρ (slopes of the Hammett plots) are listed in Table 5. For AQ, a good agreement is obtained with the previously published value (i.e.: -1.5 ± 0.17) [42]. The negative value of ρ indicates that the transition state presents an electrophilic character at the phenol reaction partner which is tuneable from PPD to AQ; it reaches a minimum with SUB this could be put in line with the evolution of the rate constants. The ρ values are very negative for the transoidal α-diketones PPD (-2.23 ± 0.15) and BZ (-2.23 ± 0.15) and should be compared with $\rho = -1.15$ for biacetyl [43]: a noticeable charge density appears and is correlated to the more pronounced aliphatic character of the carbonyl groups of biacetyl. In the flexible cisoidal diketone SUB, two factors promote a dramatic decrease of the transition state electrophilic character: (i) the absence of a strong ring constraint which still allows conjugation decoupling of the carbonyl groups from the phenyl rings, (ii) a cisoidal conformation that leads to a considerable stabilization of the resulting ketyl radical thanks to an intramolecular hydrogen bonding between the hydroxyl group and its vicinal carbonyl group (this effect has been also mentioned for camphorquinone [44] or for 1,2 aceanthrylenedione [45]). Rigid, planar and cisoid conformation is progressively enforced and accentuates the aromatic conjugation which leads to a strong delocalization of the oxygen unpaired electrons. Steric ring constraint also increases the distance between the oxygen atoms which destabilizes the corresponding ketyl radical.

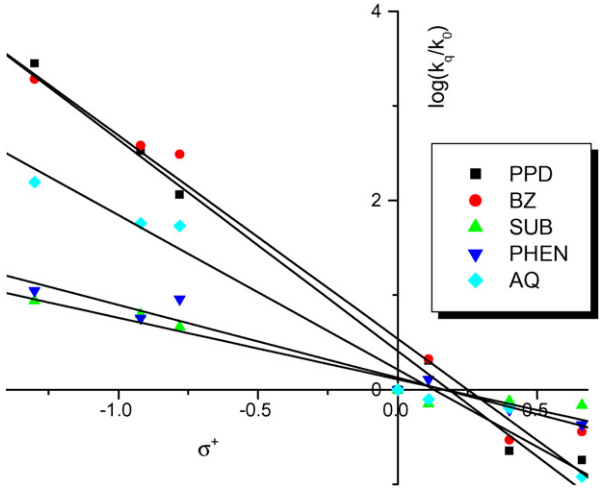

Fig. 8. Hammett plot for the hydrogen abstraction reaction of the α-diketones by the phenol derivatives in acetonitrile.

4. Conclusion

Photorotamerism related to the dihedral intercarbonyl bond of aromatic α-diketones has a strong influence on the ground state and excited state properties. The progressive decrease of the dihedral angle ϕ_{CO-CO} induces a red shift of the absorption spectrum and favours the electron acceptor ability of the α-diketones. The emitting singlet states of PPD and BZ are transoid, planar and weakly polar with a prominent n,π^* character. The triplet state of all α-diketones still conserves this n,π^* character. In the hydrogen abstraction reaction, the transient state exhibits an electrophilic character that markedly decreases when considering a flexible cisoid α-diketone. The triplet energy is both influenced by the *trans*/*cis* conformation geometry and the aliphatic character of carbonyl groups: these two parameters appear as relevant factors for the tuning of the photoreactivity of α-diketones.

References

[1] R.S. Becker, L.V. Natarajan, J. Phys. Chem. 97 (1993) 344–349.
[2] P.L. Verheijdt, H. Cerfontain, J. Chem. Soc., Perkin Trans. 2 (12) (1982) 1541–1547.
[3] J.F. Arnett, S.P.M. Glynn, J. Phys. Chem. 79 (1975) 626–629.
[4] C.W.N. Cumper, A.P. Thurston, J. Chem. Soc., Perkin Trans. 2 (1) (1972) 106–110.
[5] R.S. Becker, L.V. Natarajan, C. Lenoble, R.G. Harvey, J. Am. Chem. Soc. 110 (1988) 7163–7167.
[6] E. Charney, L. Tsai, J. Am. Chem. Soc. 93 (1971) 7123–7132.
[7] N.J. Leonard, E.R. Blout, J. Am. Chem. Soc. 72 (1950) 484–487.
[8] N.J. Leonard, P.M. Mader, J. Am. Chem. Soc. 72 (1950) 5388–5397.
[9] M.B. Rubin, R. Gleiter, Chem. Rev. 100 (2000) 1121–1164.
[10] C. Bibaut-Renauld, D. Burget, J.P. Fouassier, C.G. Varelas, J. Thomatos, G. Tsagaropoulos, L.O. Ryrfors, O.J. Karlsson, J. Polym. Sci. Part A: Polym. Chem. 40 (2002) 3171–3181.
[11] N. Shimizu, P.D. Bartlett, J. Am. Chem. Soc. 98 (1976) 4193.
[12] W.M. Nau, J.C. Scaiano, J. Phys. Chem. 100 (1996) 11360–11367.
[13] N.C.d. Lucas, M.T. Silva, C. Gege, J.C. Netto-Ferreira, J. Chem. Soc., Perkin Trans. 2 (12) (1999) 2795–2801.

[14] L. Angiolini, D. Caretti, E. Salatelli, Macromol. Chem. Phys. 201 (2000) 2646–2653.
[15] X. Allonas, J.-P. Fouassier, L. Angiolini, D. Caretti, Helv. Chim. Acta 84 (2001) 2577–2588.
[16] (a) L.A. Linden, Radiation Curing in Polymer Science and Technology, vol. 4, Elsevier Applied Science, London, 1993;
(b) Q. Wan, D. Rumpf, S.R. Schricker, A. Mariotti, B.M. Culbertson, Biomacromolecules 2 (2001) 217–222.
[17] (a) C. Bibaud-Renaud, D. Burget, J.P. Fouassier, C.G. Varelas, J. Thomatos, G. Tsagaropoulos, L.O. Ryrfors, O.J. Karlsonn, J. Polym. Sci., Part A: Polym. Chem. 40 (2002) 3171–3181;
(b) C. Grotzinger, D. Burget, J.P. Fouassier, G. Richard, O. Primel, S. Yean, Proc. RadTech. USA Int. Conf. (2006).
[18] N.J. Turro, Modern Molecular Photochemistry, vol. 1, University Science Books, Sausalito, 1991.
[19] R. lsaksson, T. Liljefors, J. Chem. Soc., Perkin Trans. 2 (9) (1983) 1351–1356.
[20] V. Galasso, G.C. Pappalardo, J. Chem. Soc., Perkin Trans. 2 (5) (1976) 574–578.
[21] R.S. Silva, D.E. Nicodem, J. Photochem. Photobiol. A: Chem. 162 (2004) 231–238.
[22] J.F. Amett, G. Newkome, W.L. Mattice, S.P. McGlynn, J. Am. Chem. Soc. 96 (1974) 4385–4392.
[23] T.R. Evans, P.A. Leermakers, J. Am. Chem. Soc. 89 (1967) 4380–4382.
[24] N.J. Leonard, A.J. Krescge, M. Oki, J. Am. Chem. Soc. 77 (1955) 5078–5083.
[25] S.R. Meech, D. Phillips, J. Photochem. 23 (1983) 193–217.
[26] M.J. Frisch, G.W. Trucks, H.B. Schlegel, G.E. Scuseria, M.A. Robb, J.R. Cheeseman, V.G. Zakrzewski, J.A. Montgomery Jr., R.E. Stratmann, J.C. Burant, S. Dapprich, J.M. Millam, A.D. Daniels, K.N. Kudin, M.C. Strain, O. Farkas, J. Tomasi, V. Barone, M. Cossi, R. Cammi, B. Mennucci, C. Pomelli, C. Adamo, S. Clifford, J. Ochterski, G.A. Petersson, P.Y. Ayala, Q. Cui, K. Morokuma, P. Salvador, J.J. Dannenberg, D.K. Malick, A.D. Rabuck, K. Raghavachari, J.B. Foresman, J. Cioslowski, J.V. Ortiz, A.G. Baboul, B.B. Stefanov, G. Liu, A. Liashenko, P. Piskorz, I. Komaromi, R. Gomperts, R.L. Martin, D.J. Fox, T. Keith, M.A. Al-Laham, C.Y. Peng, A. Nanayakkara, M. Challacombe, P.M.W. Gill, B. Johnson, W. Chen, M.W. Wong, J.L. Andres, C. Gonzalez, M. Head-Gordon, E.S. Replogle, J.A. Pople, Gaussian 98. Revision A.11, Gaussian Inc., Pittsburgh PA, 2001.
[27] (a) H.B. Klevens, J.R. Platt, J. Chem. Phys. (1949) 470;
(b) J.R. Platt, J. Chem. Phys. 17 (1949) 484.
[28] C. Libot, D. Pletcher, Electrochem. Commun. 2 (2000) 141–144.
[29] E. Lippert, Z. Naturforsch. (1955) 541.
[30] M. Rubio, M. Merchàn, E. Orti, B.O. Roos, Chem. Phys. (1994) 395.
[31] A. Bigotto, V. Galasso, G. Distefano, A. Modelli, J. Chem. Soc., Perkin Trans. 2 (11) (1979) 1502–1506.
[32] T.-S. Fang, R.E. Brown, C.L. Kwan, L.A. Singer, J. Phys. Chem. 82 (1978) 2489–2496.
[33] T.-S. Fang, L.A. Singer, J. Am. Chem. Soc. 100 (1978) 6216–6278.
[34] T.S. Fang, R.E. Brown, L.A. Singer, J. C. S. Chem. Commun. (1978) 116.
[35] H. Inoue, T. Sakurai, J. Chem. Soc., Chem. Commun. (1983) 314–315.
[36] S.V. Jovanovic, D.G. Morris, C.N. Pliva, J.C. Scaiano, J. Photochem. Photobiol. A: Chem. 107 (1997) 153–158.
[37] J. Saltiel, H.C. Curtis, L. Metts, J.W. Miley, J. Winterle, M. Wrighton, J. Am. Chem. Soc. 92 (1970) 410–411.
[38] T. Okutsu, M. Ooyama, H. Hiratsuka, J. Tsuchiya, K. Obi, J. Phys. Chem. A 104 (2000) 288–292.
[39] M.V. Encinas, P.J. Wagner, J.C. Scaiano, J. Am. Chem. Soc. 102 (1980) 1357–1360.
[40] N.J. Turro, R. Engel, J. Am. Chem. Soc. 91 (1969) 7113–7121.
[41] J. March, Advanced Organic Chemistry, Wiley-Interscience, 1985.
[42] N.C.d. Lucas, J.C. Netto-Ferreira, J. Photochem. Photobiol. A: Chem. 116 (1998) 203–208.
[43] N.J. Turro, T. Lee, J. Mol. Photochem. 2 (1970) 185–190.
[44] B.M. Monroe, S.A. Weiner, G.S. Hammond, J. Am. Chem. Soc. 90 (1968) 1913–1914.
[45] A.C.S. Serra, N.C.d. Lucas, J.C. Netto-Ferreira, J. Braz. Chem. Soc. 15 (2004) 481–486.